



HAL
open science

Enhancement under UV–visible and visible light of the ZnO photocatalytic activity for the antibiotic removal from aqueous media using Ce-doped Lu₃Al₅O₁₂ nanoparticles

Lobna Zammouri, Abdelhay Aboulaich, Bruno Capoen, Mohamed Bouazaoui, Mohamed Sarakha, Mostafa Stitou, Rachid Mahiou

► To cite this version:

Lobna Zammouri, Abdelhay Aboulaich, Bruno Capoen, Mohamed Bouazaoui, Mohamed Sarakha, et al.. Enhancement under UV–visible and visible light of the ZnO photocatalytic activity for the antibiotic removal from aqueous media using Ce-doped Lu₃Al₅O₁₂ nanoparticles. *Materials Research Bulletin*, 2018, 106, pp.162-169. hal-01823043

HAL Id: hal-01823043

<https://hal.science/hal-01823043v1>

Submitted on 15 Jul 2024

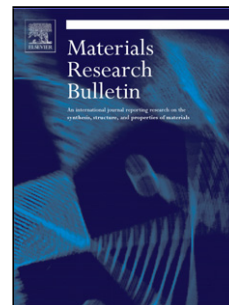
HAL is a multi-disciplinary open access archive for the deposit and dissemination of scientific research documents, whether they are published or not. The documents may come from teaching and research institutions in France or abroad, or from public or private research centers.

L'archive ouverte pluridisciplinaire **HAL**, est destinée au dépôt et à la diffusion de documents scientifiques de niveau recherche, publiés ou non, émanant des établissements d'enseignement et de recherche français ou étrangers, des laboratoires publics ou privés.

Accepted Manuscript

Title: Enhancement under UV-visible and visible light of the ZnO photocatalytic activity for the antibiotic removal from aqueous media using Ce-doped Lu₃Al₅O₁₂ nanoparticles

Authors: Lobna Zammouri, Abdelhay Aboulaich, Bruno Capoen, Mohamed Bouazaoui, Mohamed Sarakha, Mostafa Stitou, Rachid Mahiou



PII: S0025-5408(18)31235-2
DOI: <https://doi.org/10.1016/j.materresbull.2018.05.039>
Reference: MRB 10036

To appear in: *MRB*

Received date: 22-4-2018
Revised date: 30-5-2018
Accepted date: 31-5-2018

Please cite this article as: Zammouri L, Aboulaich A, Capoen B, Bouazaoui M, Sarakha M, Stitou M, Mahiou R, Enhancement under UV-visible and visible light of the ZnO photocatalytic activity for the antibiotic removal from aqueous media using Ce-doped Lu₃Al₅O₁₂ nanoparticles, *Materials Research Bulletin* (2018), <https://doi.org/10.1016/j.materresbull.2018.05.039>

This is a PDF file of an unedited manuscript that has been accepted for publication. As a service to our customers we are providing this early version of the manuscript. The manuscript will undergo copyediting, typesetting, and review of the resulting proof before it is published in its final form. Please note that during the production process errors may be discovered which could affect the content, and all legal disclaimers that apply to the journal pertain.

Enhancement under UV-visible and visible light of the ZnO photocatalytic activity for the antibiotic removal from aqueous media using Ce-doped $\text{Lu}_3\text{Al}_5\text{O}_{12}$ nanoparticles

Lobna Zammouri,^{ab} Abdelhay Aboulaich,^{b} Bruno Capoen,^c Mohamed Bouazaoui,^c Mohamed Sarakha,^b Mostafa Stitou,^a and Rachid Mahiou^{b*}*

^a Université Abdelmalek Essaadi, Faculté des Sciences de Tétouan, Laboratoire de l'Eau, d'Etude et des Analyses Environnementales, B.P. 2121 Mhannech II, 93002 Tétouan. Morocco.

^b Université Clermont Auvergne, Institut de Chimie de Clermont Ferrand UMR 6296 CNRS/UBP/Sigma Clermont, Campus des Cézeaux, TSA 60026-CS 60026, 63178, AUBIERE Cedex, France

^c Laboratoire de Physique des Lasers, Atomes et Molécules (PhLAM), CNRS (UMR 8523), CERLA/IRCICA, Université Lille 1-Sciences et Technologies, UFR de Physique, Bâtiment P5, F-59655 Villeneuve D'ASCQ cedex, France

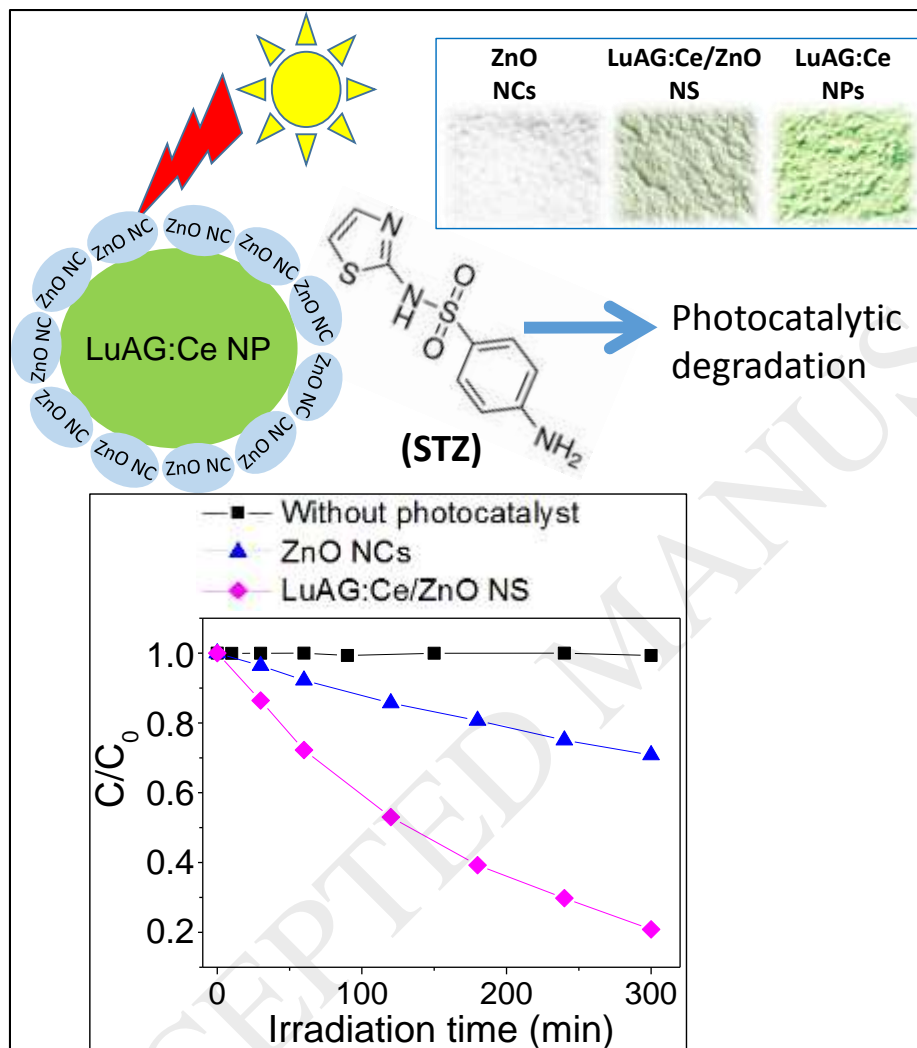
* Corresponding authors

rachid.mahiou@uca.fr

a.abdelhay@hotmail.com

Tel. 00 33 4 73 40 71 01

GRAPHICAL ABSTRACT



ABSTRACT.

We report the first synthesis of Ce-doped $\text{Lu}_3\text{Al}_5\text{O}_{12}$ Nanoparticles/ZnO Nanostructure (LuAG:Ce/ZnO NS) *via* a rapid hydrolysis/condensation of $\text{Zn}(\text{OAc})_2$ on the surface of LuAG:Ce NPs. The structural, morphological and optical properties of LuAG:Ce/ZnO NS have been fully investigated using X-Ray Diffraction (XRD), Transmission Electron Microscopy (TEM), High

Resolution Transmission Electron Microscopy (HRTEM), Energy Dispersive X-ray Spectroscopy (EDS), Fourier Transform Infrared Spectroscopy (FTIR), diffuse reflectance UV–visible spectroscopy and N₂ adsorption/desorption measurements. Results showed that ZnO Nanocrystals (ZnO NCs) of about 10 nm diameter are homogeneously grown on the surface of 100 nm LuAG:Ce NPs in a core/shell-like structure. The photocatalytic activity of the as-prepared nanostructure has been evaluated through the photodegradation of sulfathiazole (STZ), a molecule widely used as antibiotic, under UV-Vis and visible light irradiation. Results showed that STZ undergoes much higher photodegradation in the presence of LuAG:Ce/ZnO NS compared to the pure ZnO NCs under both UV-Vis and visible light. This enhanced photocatalytic capability was found to result from higher specific surface area and visible light absorption in LuAG:Ce/ZnO NS, which allowed for more surface active sites and enhanced hydroxyl radicals ($\cdot\text{OH}$) production from the nanostructured photocatalyst. The recyclability of LuAG:Ce/ZnO NS was also demonstrated.

KEYWORDS.

Nanostructured photocatalyst, visible light photocatalysis, core/shell nanostructure, nanophosphors, ZnO Nanocrystals, antibiotics, environment.

1. Introduction

The introduction of pharmaceuticals such as antibiotic agents into the aquatic environment and ecosystems was identified as one of the emerging environmental and health issues during the last two decades [1, 2]. After administration, a great portion of human and animal antibiotics is excreted partially unmetabolized or as an active metabolite and directly released in wastewater. Uncontrolled and illegal drug disposal and overuse in aquaculture might also be at the origin of

aquatic environment contamination by antibiotic agents [3]. Sulfonamides such as sulfathiazole (STZ) are an important family of antibiotics that are still commonly used in human and veterinary medicine [4-8]. For instance, sulfonamides are particularly used in livestock production and may potentially be released into the environment [9]. This result in the contamination of aquatic environment by sulfonamides resistant microorganisms and might cause a serious health and environment issues [10]. By the way, it was reported that sulfonamides are resistant to biodegradation and then may remain in the aquatic environment for a long period of time with the risk of reaching drinking water [11]. Therefore, the development of efficient and cost-effective techniques and materials to remove such pollutants from water and aquatic environment is gaining great interest today. In this context, semiconductors photocatalysis was successfully used and recognized as one of the most promising decontamination technologies. Photocatalysis is particularly attractive since it is renewable energy-based. In other words, photocatalytic removal of organic pollutants can be easily achieved under sunlight irradiation. Indeed, the absorption of the incident light by the photocatalyst triggers accelerated photochemical reactions that lead to the formation of electron-hole pairs (h^+ , e^-) and subsequent charge separation/migration/transfer which induces the production of highly reactive oxygen species (ROS) such as OH radicals ($\cdot OH$) and superoxide radicals ($\cdot O_2^-$) on the surface of the photocatalyst [12]. ROS are very strong and non-selective oxidants that are able to damage almost all kinds of organic molecules [12-13]. Due to its availability, weak toxicity, stability and relatively low cost, Titanium dioxide (TiO_2) and Zinc oxide (ZnO) semiconductors have been the most investigated semiconductor photocatalysts over the last two decades [12-18]. In particular, ZnO has been extensively studied for the removal of contaminants from water and air [19-26] and for microbial disinfection [27-28]. However, efforts are still needed to address two major issues to expand the adoption of ZnO photocatalyst in

this area. First, pure ZnO is a wide bandgap material ($E_g = 3.37$ eV at room temperature) that can only be activated by ultraviolet (UV) light, which represents only about 5% of the solar light [12]. Second, the rate of photogenerated electrons and holes recombination within ZnO crystal structure is too high, which results in low diffusion of charge carriers from the bulk to the surface of ZnO and therefore reduces the photocatalytic efficiency of the pure ZnO semiconductor [29]. In order to overcome these two issues, two approaches have been thoroughly studied in the literature. The first one consists in ZnO crystal lattice modification by doping the material with metals (Cu, Mn, Co, Al, *etc*), non-metal (C, N, S, *etc*) or rare earth elements (Ce, Gd, La, Sm, *etc*) [30-39]. The introduction of such impurities increases the material defects and makes the absorption of visible light by ZnO semiconductor possible. Furthermore, ZnO doping produces more traps for photogenerated charge carriers and thus decreases the recombination of electron-holes rate which promotes the charge diffusion from the bulk to the surface of ZnO. The second approach proposes the coupling of ZnO with other semiconductors such as Fe_2O_3 , CdS, Au, Ag_2S , Bi_2S_3 , PbS, *etc*, also called sensitizers, that generally have narrower energy band gap so that the photogenerated charge of the sensitizer can be easily injected into the ZnO conduction band [40-44]. Therefore, ZnO/Semiconductor heterostructures have more efficient charge separation which results in enhanced photocatalytic activity. Recently, light converting phosphors have also attracted significant attention for using as visible light sensitizers for ZnO. Significant efforts focused on both down-converting phosphors (DCP), which absorb light of high energy photons to emit light of lower energy photons, and up-converting phosphors (UCP), which absorb light of low energy to emit light of higher energy photons [45]. In practice, when associated with ZnO semiconductor, UCP are able to absorb NIR or visible light and then emit UV or visible light which can be easily absorbed by the semiconductor to produce more electron-hole pairs and active sites for ROS. For

instance, Er^{3+} doped YAlO_3 ($\text{YAlO}_3:\text{Er}^{3+}$) can absorb visible light at 486.5 nm and 542.4 nm and emit UV light around 318.7 nm and 320.1 nm respectively [46]. The material also showed up-conversion photoluminescence around 326–342 nm and 354–359 nm upon excitation at 657.8 nm [47]. It was found, for example, that the $\text{YAlO}_3:\text{Er}^{3+}/\text{ZnO}$ composite with 6%wt of $\text{YAlO}_3:\text{Er}^{3+}$ has higher photocatalytic degradation rate (86%) of acid red B at 60 min under solar light irradiation when compared to pure ZnO (69%) [48]. It was also demonstrated that DCP, such as $\text{Y}_3\text{Al}_5\text{O}_{12}:\text{Ce}^{3+}$, $\text{Y}_2\text{O}_2\text{S}:\text{Eu}^{3+}$, $\text{NaSrBO}_3:\text{Tb}^{3+}$ and $\text{Lu}_3(\text{Al,Si})_5(\text{O,N})_{12}:\text{Ce}^{3+}$, can effectively enhance the visible light photocatalytic activity of the wide band gap ZnO semiconductor for the removal of dyes from aqueous solution [49-53]. The enhancement of the photocatalytic performance of ZnO/DCP composite has been ascribed to two main reasons. First, the DCP is able to absorb UV or visible light (e.g. blue light) and emit visible light at longer wavelengths that can be easily absorbed by the dye (used as pollutant model). The photo-generated electrons-holes within the dye can actually lead to its self-destruction. Second, the increase of light absorption by the ZnO/DCP composite due to the high absorption of both phosphor and dye as well as the reduction of electron-hole pairs recombination could also be at the origin of the photocatalytic degradation enhancement under visible light [44, 50-52]. The contribution of the self-degradation of the dye into the photocatalytic process was already demonstrated in the literature [51]. For instance, it was found that the photocatalytic degradation rate of Methylene Blue (MB) and Rhodamine B (RhB) is much higher compared to that of Methyl Orange (MO) when ZnO/ $\text{NaSrBO}_3:\text{Tb}^{3+}$ photocatalyst is used. This is due to the fact that the emission spectrum of the $\text{NaSrBO}_3:\text{Tb}^{3+}$ phosphor (540-700nm) matches well the absorption spectra of both MB (absorption band centered at 550nm) and RhB (absorption band centered at around 650nm) while the MO only absorbs the photons with wavelength shorter than 540nm and thus cannot efficiently absorb the light emitted by the

phosphor [51]. However, the contribution of the DCP in the reduction of electron-hole pairs recombination within ZnO semiconductor is not obvious so far. This is because in most reported studies, where ZnO/light emitting phosphor composite was used as a photocatalyst, organic dyes were systematically used as a pollutant model. The study of the photocatalytic degradation of other kinds of pollutants, besides dyes, using ZnO/light emitting phosphors is however indispensable to gain better understanding of how the light emitting phosphors can enhance the photocatalytic performances of ZnO semiconductor in the visible light. By the way, to the best of our knowledge, the ZnO/DCP nanostructures have never been applied to the photocatalytic degradation of pharmaceutical substances such as antibiotics.

In the present study, we report the first synthesis of Lu₃Al₅O₁₂:Ce Nanoparticles/ZnO nanostructures (LuAG:Ce/ZnO NS) with core/shell like structure starting from LuAG:Ce NPs and zinc acetate in ethanol solvent using a simple sol-gel method. Then, the structural, morphological and optical properties of LuAG:Ce/ZnO NS have been examined using XRD, TEM, HRTEM, EDS, FTIR, diffuse reflectance UV–visible spectroscopy and BET surface area measurements. Finally, the photocatalytic efficiency of the as-prepared nanostructured photocatalyst for the degradation of STZ in both UV-Vis and visible light was evaluated and systematically compared to the pure ZnO NCs.

2. Materials and methods

2.1 Materials

Anhydrous zinc acetate (Zn(OAc)₂, 99.9%), oleic acid (> 97%, CAS number 112-80-1), tetramethyl ammonium hydroxide pentahydrate [TMAH, > 97%], sulfathiazole (98%, CAS number 72-14-0) and anhydrous ethanol were purchased from Sigma-Aldrich and used as received. Micro-sized Ce-doped Lu₃Al₅O₁₂ phosphor with an average particle size (D50) of 15 μm was purchased from Phosphor Technology (UK). Disodium terephthalate (DST, 99+%, CAS number

10028-70-3) was purchased from Alfa Easer and used as received without additional purification. All photocatalytic assays related solutions were prepared using Milli-Q water (18.2 M Ω cm, Millipore) as a solvent.

2.2 Preparation of Ce-doped Lu₃Al₅O₁₂ nanoparticles (LuAG:Ce NPs)

LuAG:Ce NPs were prepared via a top-down approach starting from commercialized micro-sized LuAG:Ce phosphor with D50 of about 15 μ m. The micro-particles were grinded using a high energy ball mill (Emax, Retsch, Germany). In a typical experiment, 10g of the micro-sized LuAG:Ce phosphor and 240 g of milling balls (with 0.5 mm diameter) were introduced into a 125mL ceramic jar. Both milling balls and jar are made of high resistant zirconia material. Then, 45mL of anhydrous ethanol solvent were added to the mixture. The jar was closed and placed into the ball mill. The particles were then grinded during 30min at a rotation speed of 1800 rpm. After grinding, the LuAG:Ce NPs were separated from the zirconia balls using a metallic sieve with a mesh size of 275 μ m. The resulting LuAG:Ce NPs suspension was stable at room temperature for several weeks.

2.3 Preparation of LuAG:Ce/ZnO NS and ZnO NCs photocatalysts

In order to allow ZnO nanocrystals (ZnO NCs) to grow on the surface of LuAG:Ce NPs, Zn(OAc)₂ and TMAH were progressively added to LuAG:Ce NPs suspension (1mg.mL⁻¹), under vigorous stirring at 100°C, as illustrated in the figure S1 (supplementary material). The Zn(OAc)₂ solution was prepared by dissolving 68mg (0.37 mmol) of anhydrous Zn(OAc)₂ in 10mL of anhydrous ethanol and mixed then with 30 μ l of oleic acid. TMAH solution was prepared by dissolving 110mg (0.61 mmol) of tetramethyl ammonium hydroxide pentahydrate in 10mL of anhydrous ethanol. LuAG:Ce NPs suspension was prepared by dispersing 30 mg of LuAG:Ce NPs powder in anhydrous ethanol at 1mg.mL⁻¹ concentration. The theoretical LuAG:Ce/ZnO weight

ratio was 1:1. $\text{Zn}(\text{OAc})_2$ and TMAH solutions injections (1mL each one) into LuAG:Ce NPs suspension have been alternated so that the hydrolysis/condensation of $\text{Zn}(\text{OAc})_2$ precursor can occur on the surface of LuAG:Ce NPs. The resulting solution was centrifuged (15 min at 4000 rpm) with removal of the supernatant and precipitate was washed several times with ethanol solvent. The collected green precipitate was then dried in air at 80°C , and finally heated in oven at 500°C for 2 hours. Pure ZnO NCs were synthesized according to the procedure described in our previous reports [53].

2.4 DST assay

The production of hydroxyl radicals ($\cdot\text{OH}$) by pure ZnO NCs and LuAG:Ce/ZnO NS was estimated using disodium terephthalate (DST), which turns into fluorescent 2-hydroxyterephthalate (2-OH-DST) emitting at 428 nm upon reaction with $\cdot\text{OH}$ radicals. Briefly, 40 mg of photocatalyst (ZnO NCs or LuAG:Ce/ZnO NS) were dispersed in 20 mL of DST aqueous solution (2×10^{-5} M). The mixture was then stirred in the dark for about 20min so that the photocatalyst is properly dispersed in the solution before being irradiated (Xe lamp with $P = 1000\text{W}$) for about 4 min. Samples have been collected at different irradiation times. The photoluminescence (PL) spectra (under 350 nm excitation) were then recorded on each sample in order to estimate the 2-OH-DST molecules formed vs time.

2.5 Photocatalytic activity

The photocatalytic activity of the as-prepared materials was studied through the degradation of sulfathiazole (STZ) in aqueous solution (10^{-4} M). In a typical experiment, 20 mg of photocatalyst were mixed with 10 mL of STZ aqueous solution to reach a photocatalyst concentration of $2 \text{ g}\cdot\text{L}^{-1}$. The mixture was then ultrasonicated for 10min (using Fisherbrand FB 15050 setup) and then stirred during 30 min in the dark in order to reach the adsorption equilibrium. We should note that

the blank experiments clearly showed that hydroxyl radicals are not formed during the sample preparation step. The photocatalyst/STZ dispersion was then transferred into the photocatalytic glass reactor and finally exposed to the Xe lamp (250 nm - 1000 nm, 1000W). The photocatalytic activity was studied under UV-Vis and Visible light. In the first study, both UV (350-400nm) and visible light (400-800nm) from the Xe lamp were used during the irradiation process. In that case, wavelengths from 250nm to 350nm were filtered using a 350nm filter while NIR light (wavelengths longer than 800nm) was filtered by water. As for the photocatalytic activity under visible light, a 400nm glass filter was used in order to cut off the wavelengths below 400nm. The light intensity at the surface of STZ solution under UV and UV-Vis irradiation was estimated to be 1.5×10^{18} photons $\text{cm}^{-2} \text{s}^{-1}$ and 5.7×10^{17} photons $\text{cm}^{-2} \text{s}^{-1}$, respectively.

The figure S2 (supplementary material) shows the transmittance curve and the light output of the Xe lamp with 350nm and 400nm glass filters. The photocatalyst/STZ mixture was continuously stirred during the light irradiation. The disappearance of STZ vs time was followed by high performance liquid chromatography (HPLC) using a Waters 540 HPLC chromatograph system equipped with a Waters 996 photodiode array detector. The experiments were performed using UV detection at 250nm and 300nm. The flow rate was $1.0 \text{ ml} \cdot \text{min}^{-1}$ and the injected volume was $50 \mu\text{l}$. The elution was accomplished with acidified water (0.1% acetic acid) and methanol (40:60 v/v ratio). The photocatalyst/STZ solutions collected at different irradiation times were centrifuged and only the supernatant was analyzed by HPLC. The byproducts obtained through the photocatalytic decomposition process of STZ were analyzed by high-performance liquid chromatography/electrospray ionization/mass spectrometry (HPLC/ESI/MS) in positive mode. We should add that all the photocatalysis related experiments were repeated two times at least and experiments were found to be reproducible with an error of about 5%.

2.6 Characterization methods

XRD patterns were recorded on a Philips X-Pert Pro diffractometer operating with the Cu-K α radiation ($\lambda = 1.5406 \text{ \AA}$). An ATR accessory installed on a Nicolet FT-IR spectrometer was used to record FTIR spectra. The particle size and morphology was investigated by means of a Hitachi H-7650 Transmission Electron Microscope (TEM) operating at 80 kV, in a high resolution mode and combined with a Hamamatsu AMT HR CCD camera placed in a side position. High Resolution Transmission Electron Microscope (HRTEM) observations were performed using a FEI Tecnai G2 20 instrument operating at 200 kV coupled with Energy-Dispersive X-ray Spectroscopy (EDS) measurements for chemical identification. TEM and HRTEM images were taken by depositing a drop of the photocatalyst dispersion in ethanol onto a carbon film supported nickel grid. In order to characterize the porosity of the synthesized materials, nitrogen sorption isotherms were recorded at 77.35 K using a MICROMERITICS ASAP 2020 automatic apparatus, after an outgassing process of 12 hours at 90 °C under secondary vacuum. The specific surface area was determined by the Brunauer–Emmett–Teller (BET) method [54]. The pore size distribution and volume were obtained from the N₂ desorption/isotherm using the Barrett–Joyner–Halenda (BJH) model [55]. LuAG:Ce NPs suspensions in ethanol were also studied in terms of particle size distribution using Dynamic Light Scattering (DLS) method. Zetasizer Nano ZS, Malvern, UK instrument was used for measurements. Diffuse reflectance UV–vis spectra of the samples were measured using a Shimadzu UV-2101PC spectrophotometer. BaSO₄ is used as a standard for base line measurements and spectra are recorded in the 300nm – 800nm spectral range.

3. Results and discussion

3.1 Preparation of Ce-doped Lu₃Al₅O₁₂ Nanoparticles (LuAG:Ce NPs)

LuAG:Ce NPs have been prepared by a “top-down” approach, starting from commercialized LuAG:Ce microparticles phosphor, using high energy ball milling method. The ball milling conditions (LuAG:Ce phosphor concentration vs ethanol, rotation speed, milling time, *etc*) have been adjusted to yield LuAG:Ce NPs with narrow particle size distribution as shown in figure 1(a). Results also showed that the DLS particle size was about 200nm which is two times larger than the average particle diameter measured from the TEM image (*i.e.* 100 nm). A representative TEM image of the as-prepared LuAG:Ce particles is given in figure 1(b). This is because the DLS particle size corresponds to the hydrodynamic diameter which includes both the size of the particle core and the thickness of the solvation layer surrounding the particle. Moreover, TEM image of LuAG:Ce NPs taken at higher magnification (figure S6, supplementary materials) showed well dispersed nanoparticles with irregular shape and size since LuAG:Ce NPs are formed by breaking up the initial LuAG:Ce particles due to the high energy ball milling process.

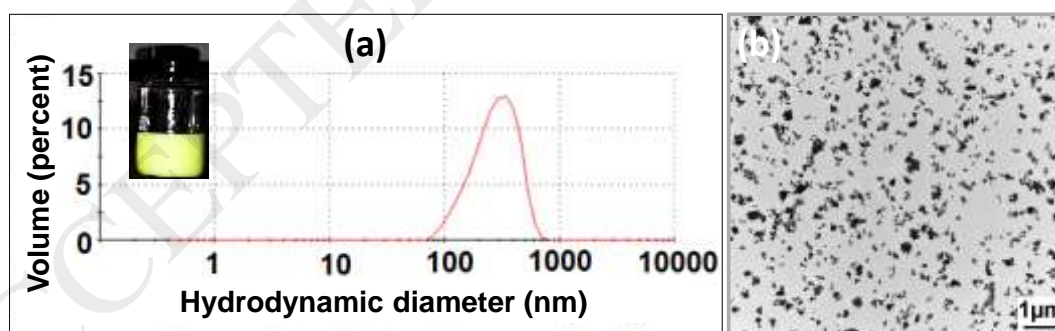


Figure 1. Particles size distribution measured by DLS (a) and a representative TEM image of the as-prepared LuAG:Ce NPs (b). Inset of figure 1(a) is a picture of the as-prepared LuAG:Ce suspension in ethanol.

TEM observation of the as-prepared LuAG:Ce NPs also revealed the presence of relatively well dispersed nanoparticles with low degree of agglomeration. The inset of figure 1(a) shows a picture of the as-prepared green LuAG:Ce NPs dispersion that was stable for few weeks. This result indicates that the high energy ball milling method is suitable for making stable phosphor nanoparticles. The crystallinity of the as-prepared LuAG:Ce NPs was demonstrated by XRD as shown in figure S3 (supplementary material). All diffraction peaks correspond to the pure $\text{Lu}_3\text{Al}_5\text{O}_{12}$ phase (JCPDS file 73-1368) indicating that the high ball milling doesn't alter the original structure of LuAG. Moreover, no contamination with zirconia was observed. XRD patterns also showed broader XRD in the case of LuAG:Ce NPs compared to the commercialized LuAG:Ce microparticles. The broader XRD peaks are consistent with the formation of LuAG:Ce NPs as shown by TEM (figure 1(b)). The crystallite size of LuAG:Ce NPs can be estimated from the full-width at half maximum (FWHM) of the XRD peaks using the Debye-Scherrer's equation [56]. The crystallite size was found to be around 100 nm which is in agreement with the TEM result.

3.2 Synthesis of $\text{Lu}_3\text{Al}_5\text{O}_{12}$:Ce NPs/ZnO Nanostructures (LuAG:Ce/ZnO NS)

The structure of the as-prepared LuAG:Ce/ZnO composites was first studied by XRD as shown in figure 2.

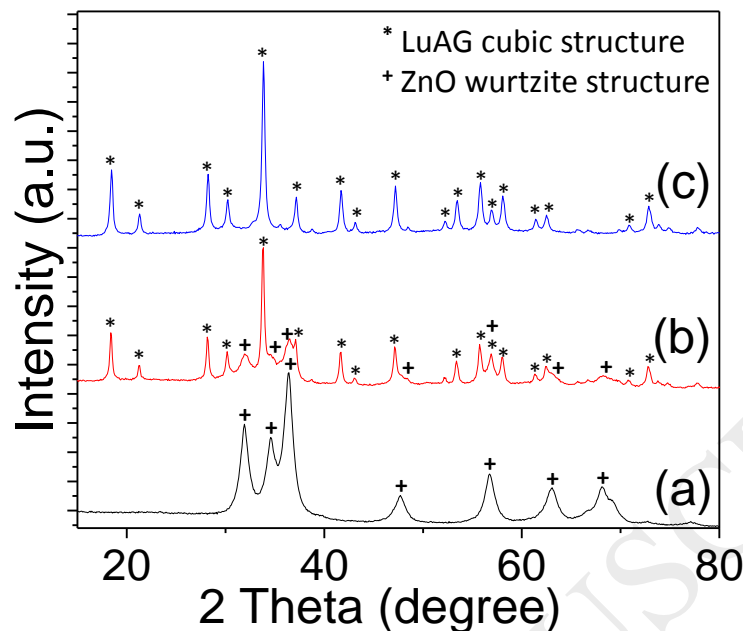


Figure 2. XRD pattern of (a) Pure ZnO NCs (b) LuAG:Ce/ZnO NS and (c) pure LuAG:Ce NPs

The XRD of LuAG:Ce NPs and ZnO NCs are also provided for comparison. From the XRD patterns, it can be seen that all the samples are well crystallized. As for pure ZnO NCs, the appearance of diffraction peaks corresponding to (100), (002), (101), (102), (110), (103), and (200) planes indicates the hexagonal wurtzite structure (JCPDS Card No. 80-0075) of ZnO. The broadening of the ZnO diffraction peaks is due to the small particle diameter of ZnO NCs. The crystallite size was found to be about 10 nm using Debye Scherrer formula. This value is in agreement with the particle size measured from TEM images.

The XRD pattern of LuAG:Ce/ZnO NS shows the presence of diffraction peaks of both LuAG:Ce NPs and ZnO NCs suggesting that the presence of the LuAG:Ce NPs in the reaction medium, during synthesis, doesn't compromise the formation of well crystallized ZnO NCs.

In order to confirm the formation of LuAG:Ce/ZnO NS and investigate the morphology, particles size, structure as well as the chemical composition of the composites, the as-prepared LuAG:Ce/ZnO NS was observed by TEM and HRTEM coupled with EDS measurements. TEM

observation (figure S4, supplementary material) showed a relatively well dispersed nanoparticles of about 100 nm surrounded with a shell of smaller and lower density nanoparticles of about 10 nm diameter. One representative particle from figure S4 was selected and analyzed with EDS as shown in figure 3(a).

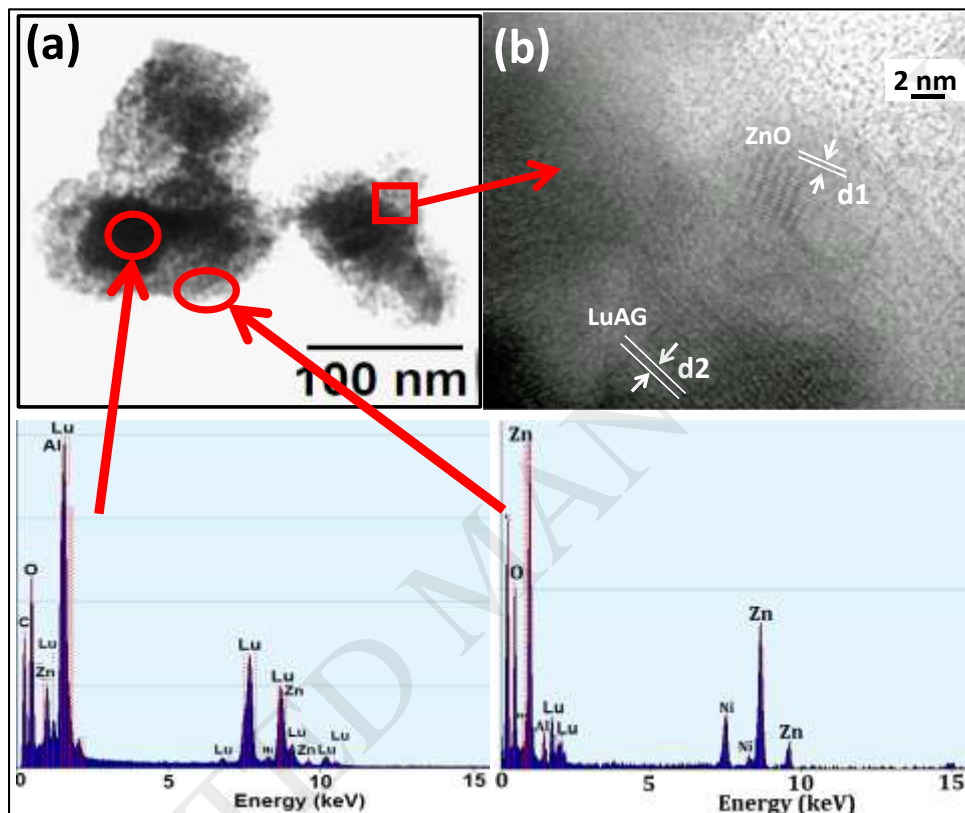


Figure 3. (a) TEM image of a representative LuAG:Ce/ZnO nanoparticles with the corresponding EDS spectra and (b) HRTEM image taken at the LuAG:Ce/ZnO interface.

The EDS spectra revealed that the core of the particle is enriched with LuAG elements while the shell of the particle is dominated by Zn and O elements. We should note that the Ni peaks in the EDS spectra are due to the Ni-based grids used for TEM/EDS analysis. In addition, a representative HRTEM image (figure 3(b)) taken at the core/shell interface of the particle shows the distance between the adjacent lattice fringes within the core and the periphery of the particle to be 4.8 Å (d2) and 2.81 Å (d1), respectively. These values are consistent with the spacing of (211) planes in

the LuAG cubic structure and (100) planes in the ZnO hexagonal wurtzite structure, respectively. This result confirms the formation of LuAG:Ce NPs/ZnO nanostructure where LuAG:Ce NPs are surrounded with a shell of ZnO NCs. By the way, FTIR spectrum of LuAG:Ce/ZnO NS (figure S5, supplementary material) showed that the characteristic peaks of LuAG:Ce (801cm^{-1} , 736cm^{-1} , 702cm^{-1}) are shifted to higher wavenumbers in LuAG:Ce/ZnO NS compared to the pure LuAG:Ce NPs which suggests that the ZnO NCs would be strongly linked to the surface of LuAG:Ce NPs probably through a Zn-O-M covalent bonds (with $M=\text{Al}$, Lu). The creation of strongly linked LuAG:Ce/ZnO composite would be highly beneficial for enhancing the photogeneration/separation of e^-/h^+ carrier which could improve the photocatalytic activity of the ZnO under the visible light.

Diffuse reflectance UV-Vis spectra of the as-prepared pure ZnO NCs, LuAG:Ce NPs and LuAG:Ce/ZnO NS are presented in Figure 4. The photograph of the corresponding nanopowders are also provided in the inset of figure 4.

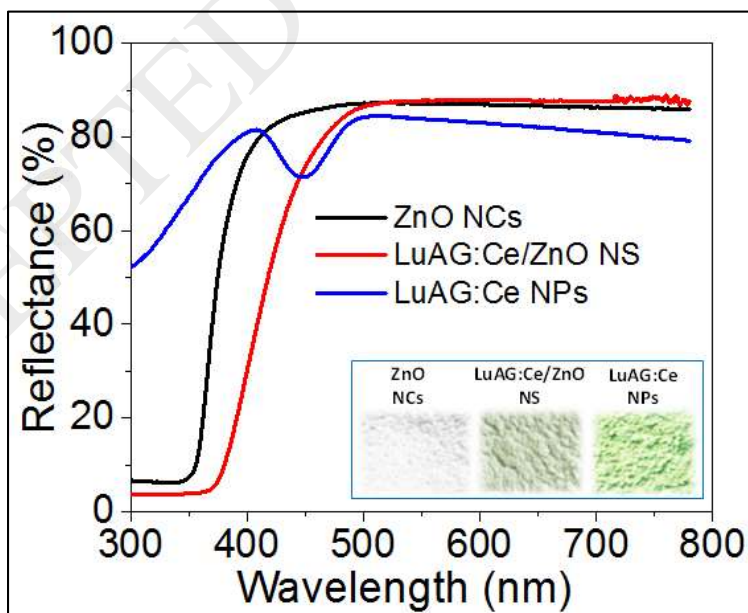


Figure 4. Diffuse reflectance UV-Vis spectra of pure ZnO NCs, LuAG:Ce NPs and LuAG:Ce/ZnO NS. Inset shows a digital picture of the corresponding nanopowders.

It can be seen from figure 4 that ZnO NCs have no absorption in the visible light due to its wide band gap. However, when ZnO NCs are associated with LuAG:Ce NPs in LuAG:Ce/ZnO core/shell NS its absorption edge seems significantly red-shifted compared to the pure ZnO NCs. The LuAG:Ce/ZnO NS reveals extended optical absorption in the 400-550nm range compared to the pure ZnO NCs. This extended optical absorption to the visible light suggests that LuAG:Ce NPs could enhance the visible light photocatalytic activity of ZnO semiconductor.

The porosity, which is one of the key parameters in photocatalysis, of the as-prepared LuAG:Ce/ZnO NS was also measured using N₂ adsorption/desorption method. The resulting N₂ adsorption/desorption isotherm of pure ZnO NCs and LuAG:Ce/ZnO NS is provided in figure 5.

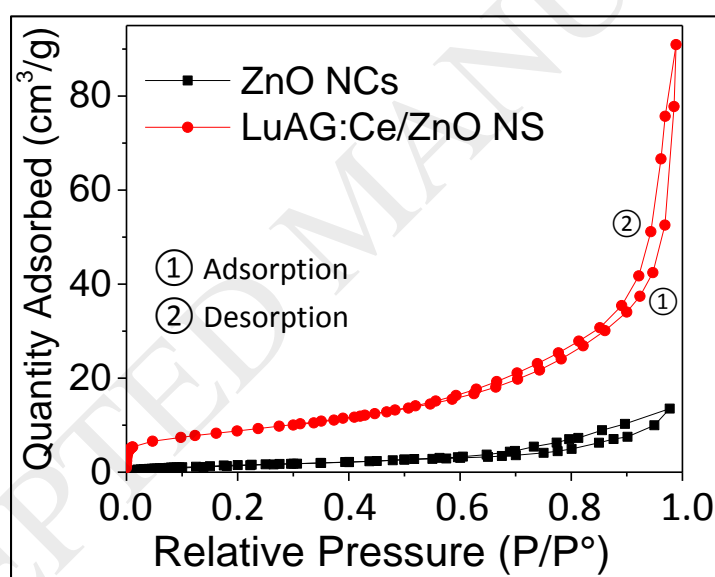


Figure 5. N₂ adsorption/desorption isotherm of the pure ZnO NCs and LuAG:Ce/ZnO NS

It can be seen that both pure ZnO NCs and LuAG:Ce/ZnO NS have a type IV isotherm with H₂ hysteresis loop according to the IUPAC classification [57], which is characteristic of mesoporous materials. Since ZnO and LuAG:Ce nanoparticles are a non-porous materials, the mesopores are likely due to the formation of interparticle cavities which result from drying/agglomeration of the corresponding particles in the nanopowder. This feature does not exhibit any limiting adsorption

at high P/P^0 and is typically observed in the literature when aggregates of nanoparticles with irregular shapes and morphologies are formed [56-59]. Figure 5 also shows that the quantity of N_2 adsorbed in LuAG:Ce/ZnO NS is much higher suggesting higher specific surface area compared to the pure ZnO NCs. Table 1 provides the BET surface area and pore volume obtained for the pure ZnO NCs, LuAG:Ce NPs and LuAG:Ce/ZnO NS.

Photocatalyst	Specific surface area ($m^2.g^{-1}$)	Pore volume ($cm^3.g^{-1}$)
ZnO NCs	6.2	0.018
LuAG:Ce NPs	40	0.2
LuAG:Ce/ZnO NS	32	0.12

Table 1. Specific surface area and pore volume of ZnO NCs, LuAG:Ce NPs and LuAG:Ce/ZnO NS.

As can be seen from the table 1, the specific surface area of LuAG:Ce/ZnO NS is $32 m^2.g^{-1}$, which is about 5 times higher compared to the pure ZnO NCs. The pore volume was also found to be about 6 times higher compared to the pure ZnO NCs. The low surface area and pore volume of the pure ZnO NCs is likely due to the fact that the original small ZnO NCs fuse together after drying/calcination to produce large and dense particles that have low interparticle cavities with mesoporous dimensions. This was supported by TEM observations performed on ZnO NCs before and after $500^\circ C$ treatment (Figure S7). The initial ZnO NCs (figure S7(a)) showed well dispersed spherical nanoparticles of about 10nm diameter with a highly homogeneous morphology and size while TEM image of the as-prepared ZnO NCs (figure S7(b)) showed much bigger aggregated

nanoparticles of about 100-200nm with inhomogeneous morphology and size. In contrast, the higher surface area and pore volume measured for LuAG:Ce/ZnO NS suggests that the growth of ZnO NCs on the surface of LuAG:Ce NPs prevents the particles from high aggregation and helps ZnO NCs to be homogeneously dispersed in the composite. This could result in much less NCs aggregates and provides more surface area and higher pore volume to the composite. It was also found that LuAG:Ce NPs have higher surface area (*i.e.* $40 \text{ m}^2 \cdot \text{g}^{-1}$) compared to LuAG:Ce/ZnO NS. Interestingly, LuAG:Ce/ZnO photocatalyst NS has an intermediate surface area between those of pure ZnO NCs and pure LuAG:Ce NPs. The lower surface area of LuAG:Ce/ZnO NS (*i.e.* $32 \text{ m}^2/\text{g}$) compared to the pure LuAG:Ce NPs (*i.e.* $40 \text{ m}^2/\text{g}$) is likely due to the fact that the growth of ZnO NCs on the surface of LuAG:Ce NPs results in core/shell like structure with bigger particle size. The aggregation of ZnO NCs in the interparticle cavities (mesopores type) formed between the LuAG:Ce NPs could also contribute to the surface area drop within the LuAG:Ce/ZnO NS. Based on these results, the LuAG:Ce/ZnO NS is supposed to yield higher photocatalytic activity. In order to check how consistent is this statement, the photocatalytic efficiency of the as-prepared ZnO NCs and LuAG:Ce/ZnO NS photocatalysts was evaluated through the photocatalytic degradation of STZ under UV-Vis and visible light.

3.3 Photocatalytic activity and recyclability studies

Figure 6 provides the kinetic of degradation of STZ with and without the presence of pure LuAG:Ce NPs, pure ZnO NCs and LuAG:Ce/ZnO NS. The C/C_0 ratio was used to represent the degradation rate, where C and C_0 are the STZ concentration at times t and 0 , respectively. C_0 was $1 \times 10^{-4} \text{ M}$ while C was calculated by integrating the area under the HPLC signal at about 6.7min, which corresponds to the retention time of STZ molecule.

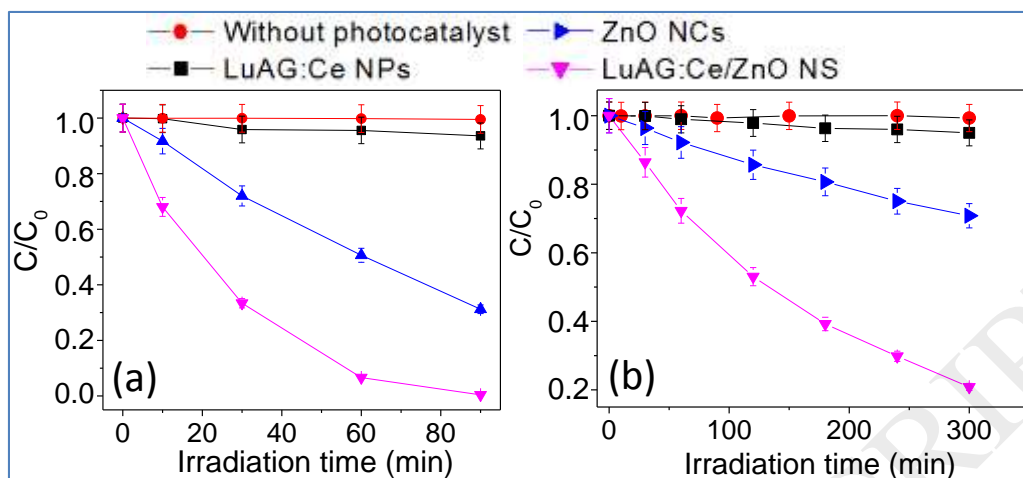


Figure 6. Evolution of STZ conversion (C/C_0) vs irradiation time under (a) UV-Visible and (b) visible light. Error bar of 5% is included.

Table 2. Initial photocatalytic reaction rate (ν) of the degradation of STZ in UV-Vis and visible light using the as-prepared photocatalysts. ν was calculated from the slope of the best-fit line through the plotted C (concentration of STZ) vs irradiation time.

Results showed first that STZ doesn't undergo any degradation in the absence of photocatalyst even though the molecule is irradiated with UV-Vis or visible light over a long period of time. Results also showed that the degradation of STZ is very slow when only pure LuAG:Ce NPs are used. However, significant and rapid degradation of STZ was observed in the presence of LuAG:Ce/ZnO NS and ZnO NCs. Interestingly, it can be seen that the photocatalytic decomposition of the STZ molecule is much higher with LuAG:Ce/ZnO NS compared to the pure ZnO NCs regardless of whether the UV-Vis or visible light irradiation is used, although the degradation rate is much higher under UV-visible light when compared to visible light. For instance, the decomposition of STZ under UV-Vis light in the presence of LuAG:Ce/ZnO NS was

Photocatalyst	Initial photocatalytic reaction rate in UV-Visible range (mol.L ⁻¹ .min ⁻¹)	Initial photocatalytic reaction rate in Visible range (mol.L ⁻¹ .min ⁻¹)
LuAG:Ce NPs	2.33 10 ⁻⁸	-
ZnO NCS	9.44 10 ⁻⁷	1.3 10 ⁻⁷
LuAG:Ce NPs/ZnO NS	3.2 10 ⁻⁶	4.62 10 ⁻⁷

found to be almost 100% at 90min while the degradation was limited to 69% when pure ZnO NCs are used. Under visible light, the decomposition of STZ in the presence of LuAG/ZnO NS reaches more than 80% at 300min, while only about 30% degradation is achieved with ZnO NCs at the same irradiation time.

Table 2 also shows that the initial photocatalytic reaction rate is about 3.5 times higher with LuAG:Ce/ZnO NS compared to the pure ZnO NCs in both UV-visible and visible light. This result clearly indicates that the introduction of LuAG:Ce NPs enhances the visible light photocatalytic response of ZnO NCs. This result is also consistent with the specific surface area measurements which showed higher surface area for LuAG:Ce/ZnO NS. In fact, higher surface area provides more adsorption active sites for the pollutant and thus facilitates the oxidation of the pollutant molecule by a direct reaction with the photo-induced holes at the surface of the photocatalyst [45]. Furthermore, it has been reported that hydroxyl radicals ($\cdot\text{OH}$) are the key trigger of the photocatalytic decomposition of STZ in aqueous media [60]. The degradation pathway would likely start with the attack of STZ benzene ring by $\cdot\text{OH}$ radicals with the generation of NH_4^+ in the medium which results in a series of reactions leading to the ring opening and the formation of a mixture of carboxylic and dicarboxylic acids [60]. In order to demonstrate the formation of hydroxyl radicals ($\cdot\text{OH}$) from LuAG:Ce/ZnO NS during the photocatalysis process, the $\cdot\text{OH}$ radical-specific fluorimetric assay was used. In this assay, $\cdot\text{OH}$ radicals have been revealed by the reaction of disodium terephthalate (DST) with the photogenerated $\cdot\text{OH}$ radicals to form the fluorescent 2-hydroxyterephthalate anion (2-OH-DST), which emits at 428nm under UV excitation [61-62]. The PL intensity at 428nm can then be correlated with the number of $\cdot\text{OH}$ radicals produced by the photocatalyst. Figure

7(a) shows the change in the relative PL intensity at 428nm of DST aqueous solutions containing ZnO NCs and LuAG:Ce/ZnO NS as a function of irradiation time.

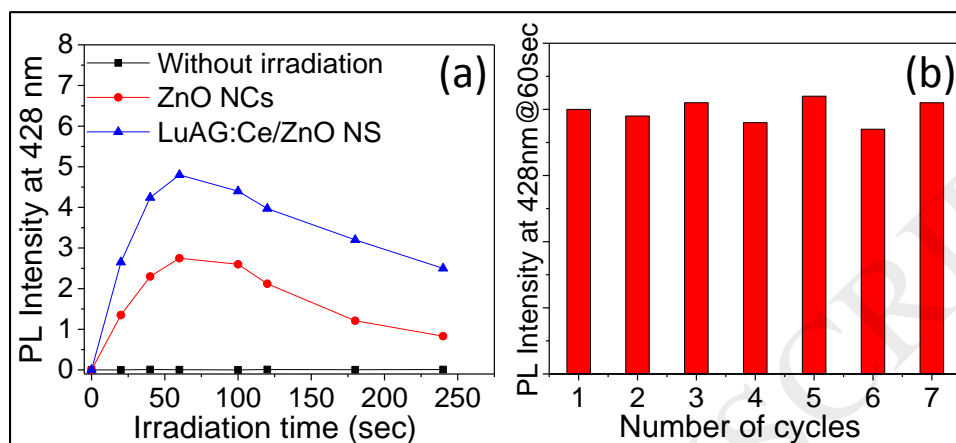


Figure 7. (a) Change in the relative PL intensity at 428nm of DST aqueous solution (2×10^{-5} M) containing ZnO NCs and LuAG:Ce/ZnO NS as a function of irradiation time and (b) photocatalytic recyclability study with LuAG:Ce/ZnO NS. Experiments were performed under UV-Vis light irradiation.

It was found that the fluorescence intensity at 428nm increases very quickly in the 60 first seconds of irradiation, which suggests a very fast production of $\cdot\text{OH}$ radicals in the medium. These results also show that LuAG:Ce/ZnO NS induces enhanced production of $\cdot\text{OH}$ radicals when compared to the pure ZnO NCs. We should add that 2-OH-DST was not produced in control experiments performed without irradiation, which confirms that the hydroxylation of DST molecule only occurs when the solution is irradiated. In other words, the production of $\cdot\text{OH}$ radicals is photo-induced. Therefore, the DST assay confirms the key role of $\cdot\text{OH}$ radicals in the photocatalytic conversion of STZ.

Moreover, by following the STZ disappearance using LuAG:Ce/ZnO NS photocatalyst, the main decomposition products were detected and identified using HPLC/ESI/MS in positive mode (figure S8, supplementary materials). At the early stages of the irradiation, with about 25% STZ

conversion, two isomer products at $m/z = 272.0172$ corresponding to the elemental composition $C_9H_{10}N_3O_3S_2$ with an error of 3.1 ppm were formed. These products likely result from the hydroxylation of STZ. Together with these two products, the analyses clearly showed the formation of small amount of 4-hydroxy-N-(1,3 thiazol) benzenesulfonamide with $m/z = 257.0049$ ($C_9H_9N_2O_3S_2$ with an error of 2.2 ppm) in perfect agreement with published results [60]. It should be noted that two other byproducts arising from the scission of S-N bond were also observed ($m/z = 174.0226$ and $m/z = 87.0140$, *data not provided*) as commonly reported with sulfonylureas compounds [63]. All these compounds represent the very first products of the photocatalytic mineralization process of STZ.

The DST assay was also used to assess the ability of reusing LuAG:Ce/ZnO NS in photocatalysis by performing consecutive DST conversion with the same LuAG:Ce/ZnO NPs batch. The photocatalyst was systematically washed several times with water in order to remove the by-products of DST conversion and traces of 2-OH-DST or DST left from the previous DST conversion trial. The recyclability of LuAG:Ce/ZnO NS was monitored by measuring the PL intensity at 428nm after 60sec irradiation for each DST conversion cycle. The results of these experiments are shown in figure 7(b). Results showed that the initial PL intensity at 428nm due to the photogenerated 2-OH-DST was maintained for up to 7 DST conversion cycles, which suggests a stable production of $\cdot OH$ radicals after each DST conversion/washing cycle. Similar results were obtained by following the STZ degradation. The good $\cdot OH$ radicals production stability observed throughout the DST conversion as well as STZ disappearance assay clearly indicates that recycling has no significant impact on the dispersion of the photocatalyst particles in the medium or on its surface properties and reactivity. This result suggests that LuAG:Ce/ZnO NS photocatalyst is

highly robust and can potentially be reused in water decontamination for many times while keeping high photocatalytic activity.

4. Conclusions

In summary, LuAG:Ce/ZnO NS photocatalyst has been successfully prepared, for the first time, using a rapid hydrolysis/condensation of $\text{Zn}(\text{OAc})_2$ in the presence of LuAG:Ce NPs. LuAG:Ce NPs of about 100 nm diameter have been easily made using ball milling method starting from standard and commercially available LuAG:Ce phosphor. The results showed that small and highly crystallized ZnO NC of about 10 nm diameter are formed and closely linked to the surface of LuAG:Ce NPs as a core/shell like structure. This structure was found to be highly beneficial for photocatalytic activity enhancement of ZnO NCs under UV-visible and visible light. The photocatalytic efficiency improvement with LuAG:Ce/ZnO NS was demonstrated through the photocatalytic decomposition of STZ in aqueous solution. Results showed that the decomposition of STZ under UV-Vis light in the presence of LuAG:Ce/ZnO NS was almost 100% at 90min while the degradation remains limited to 69% when pure ZnO NCs are used. Under visible light, the decomposition of STZ by LuAG:Ce/ZnO NS reaches more than 80% at 300min, while only about 30% degradation is achieved with ZnO NCs at the same irradiation time. The photocatalytic activity enhancement was found to be consistent with the higher specific surface area and enhanced $\cdot\text{OH}$ radicals production with LuAG:Ce/ZnO NS when compared to the pure ZnO NCs. The photocatalytic recyclability study also showed that LuAG:Ce/ZnO NS can be reused in a multiple photocatalytic cycles without compromising the photocatalytic efficiency of the composite. This feature is highly desired in photocatalysis-based water decontamination and would make LuAG:Ce/ZnO NS a very good photocatalyst in the future in that particular area.

Supplementary Material. S1: A schematic illustration of the synthetic method of LuAG:Ce/ZnO NS. **S2:** Transmittance curve and the light output of the Xe lamp with 350nm and 400nm glass filters. **S3:** XRD pattern of commercialized LuAG:Ce phosphor and as-prepared LuAG:Ce NPs. **S4:** TEM image of LuAG:Ce/ZnO NS. **S5:** FTIR spectra of ZnO NCs, LuAG:Ce NPs and LuAG:Ce/ZnO NS. **S6:** TEM image of the as-prepared LuAG:Ce NPs. **S7:** TEM image of ZnO NC before and after 500°C calcination. **S8:** Mass spectra recorded during the early stage of STZ decomposition using HPLC/ESI+/MS.

ACKNOWLEDGMENT. Authors thank Christelle Blavignac (CICS, Université d'Auvergne) for TEM observations.

REFERENCES

- [1] K. Kummerer, *Pharmaceuticals in the environment. Sources, fate, effects and risks*, Springer-Verlag: Heidelberg, 2001.
- [2] K. Kummerer, *Antibiotics in the aquatic environment – A review – Part I*, *Chemosphere* 75, (2009) 417-434.
- [3] A. B. Caracciolo, E. Topp, P. Grenni, *Pharmaceuticals in the environment: Biodegradation and effects on natural microbial communities. A review*, *J. Pharm. Biomed. Anal.* 106 (2015) 25–36.
- [4] P. Sukul, M. Spitteler, *Sulfonamides in the environment as veterinary drugs*. *Environ Contam Toxicol.* 187 (2006) 67-101.
- [5] W. Baran, J. Sochacka, W. Wardas, *Toxicity and biodegradability of sulfonamides and products of their photocatalytic degradation in aqueous solutions*, *Chemosphere* 65 (2006) 1295–1299.

- [6] J. Ziemiańska, E. Adamek, A. Sobczak, I. Lipska, A. Makowski, W. Baran, The study of photocatalytic degradation of sulfonamides applied to municipal wastewater. *Physicochem Probl Miner Process.* 45 (2010) 127-140.
- [7] W. Baran, E. Adamek, J. Ziemiańska, A. Sobczak, Effects of the presence of sulfonamides in the environment and their influence on human health. *J Hazard Mater.* 196 (2011) 1–15.
- [8] K. Hruska, M. Franek, Sulfonamides in the environment: a review and a case report. *Vet Med.* 57 (2012) 1–35.
- [9] C. Holtslander, Environmental contamination of ecosystems from antibiotic use in livestock production. Petition addressed to the auditor general of Canada, http://www.oag-bvg.gc.ca/internet/English/pet_190_e_28926.html (Accessed 11 November 2017).
- [10] V. I. Enne, D. M. Livermore, P. Stephens, L. M. Hall, Persistence of sulfonamide resistance in *Escherichia coli* in the UK despite national prescribing restriction, *Lancet* 357 (2001) 1325–1328.
- [11] B. Halling-Sorensen, S. Nors Nielsen, P. F. Lanzky, F. Ingerslev, H. C. Holten Lützhof, S. E. Jorgensen, Occurrence, fate and effects of pharmaceutical substances in the environment—a review. *Chemosphere* 36 (1998) 357–393.
- [12] M. R. Hoffmann, S. T. Martin, W. Choi, D. W. Bahnemann, Environmental Applications of Semiconductor Photocatalysis, *Chem Rev.* 95 (1995) 69–96.
- [13] L. Brunet, D. Y. Lyon, E. M. Hotze, P. J. J. Alvarez, M. R. Wiesner, Comparative Photoactivity and Antibacterial Properties of C60 Fullerenes and Titanium Dioxide Nanoparticles, *Environ Sci Technol.* 43 (2009) 4355–4360.

- [14] S. Y. Pung, W. P. Lee, A. Aziz, Kinetic Study of Organic Dye Degradation Using ZnO Particles with Different Morphologies as a Photocatalyst, *Int J Inorg Chem.* 2012 (2012) 1-9.
- [15] J. Wang, Z. Wang, B. Huang, Y. Ma, Y. Liu, X. Qin, X. Zhang, Y. Dai, Oxygen Vacancy Induced Band-Gap Narrowing and Enhanced Visible Light Photocatalytic Activity of ZnO, *ACS Appl Mater Interfaces* 4 (2012) 4024–4030.
- [16] S. Pekárek, J. Mikeš, J. Krýsa, Comparative study of TiO₂ and ZnO photocatalysts for the enhancement of ozone generation by surface dielectric barrier discharge in air, *Appl Catal A*, 502 (2015) 122–128.
- [17] A. Fujishima, T. N. Rao, D. A. Tryk, Titanium dioxide photocatalysis, *J Photochem Photobiol C: Photochem Rev.* 1 (2000) 1-21.
- [18] T. Matsunaga, M. Okoch, TiO₂-Mediated Photochemical Disinfection of Escherichia coli Using Optical Fibers, *Environ Sci Technol.* 29 (1995) 501-505.
- [19] R. M. Thankachan, N. Joy, J. Abraham, N. Kalarikkal, S. Thomas, O. S. Oluwafemi, Enhanced photocatalytic performance of ZnO nanostructures produced via a quick microwave assisted route for the degradation of rhodamine in aqueous solution, *Mater. Res. Bull.* 105 (2018) 63-67.
- [20] G. Marci, V. Augugliaro, M. J. Lopez-Munoz, C. Martin, L. Palmisano, V. Rives, M. Schiavello, R. J. D. Tilley, A. M. Venezia, Preparation Characterization and Photocatalytic Activity of Polycrystalline ZnO/TiO₂ Systems. 2. Surface, Bulk Characterization, and 4-Nitrophenol Photodegradation in Liquid–Solid Regime, *J Phys Chem B.* 105 (2001) 1033–1040.

- [21] Y. Liu, C. Xu, Z. Zhu, J. Lu, A. G. Manohari, Z. Shi, Self-assembled ZnO/Ag hollow spheres for effective photocatalysis and bacteriostasis, *Mater. Res. Bull.* 98 (2018) 64-69.
- [22] N. Sabana, M. Swaminathan, The effect of operational parameters on the photocatalytic degradation of acid red 18 by ZnO, *Sep Purif Technol.* 56 (2007) 101–107.
- [23] F. Xu, P. Zhang, A. Navrotsky, Z. Y. Yuan, T. Z. Rent, M. Halasa, B. L. Su, Hierarchically Assembled Porous ZnO Nanoparticles: Synthesis, Surface Energy and Photocatalytic Activity, *Chem Mater.* 19 (2007) 5680–5686.
- [24] H. Zeng, W. Cai, P. Liu, X. Xu, H. Zhou, C. Klingshirm, H. Kalt, ZnO-Based Hollow Nanoparticles by Selective Etching: Elimination and Reconstruction of Metal–Semiconductor Interface, Improvement of Blue Emission and Photocatalysis, *ACS Nano* 2 (2008) 1661–1670.
- [25] C. Yang, J. Yu, Q. Li, Y. Yu, Facile synthesis of monodisperse porous ZnO nanospheres for organic pollutant degradation under simulated sunlight irradiation: The effect of operational parameters, *Mater. Res. Bull.* 87 (2017) 72-83.
- [26] Y. Hong, C. Tian, B. Jiang, A. Wu, Q. Zhang, G. Tian, H. Fu, Facile synthesis of sheet-like ZnO assembly composed of small ZnO particles for highly efficient photocatalysis, *Mater Chem A.* 1 (2013) 5700–5708.
- [27] R. J. Barnes, R. Molina, J. Xu, P. J. Dobson, I. P. Thompson, Comparison of TiO₂ and ZnO nanoparticles for photocatalytic degradation of methylene blue and the correlated inactivation of gram-positive and gram-negative bacteria, *J Nanopart Res.* 15 (2013) 1432–1443.

- [28] K. Rekha, N. Nirmala, M. G. Nair, A. Anukaliani, Structural, optical, photocatalytic and antibacterial activity of zinc oxide and manganese doped zinc oxide nanoparticles, *Physica B: Condensed Matter* 405 (2010) 3180–3185.
- [29] B. Chouchene, T. Ben Chaabane, L. Balan, E. Girot, K. Mozet, G. Medjahdi, R. Schneider, High performance Ce-doped ZnO nanorods for sunlight-driven photocatalysis, *Beilstein J Nanotechnol.* 7 (2016) 1338–1349.
- [30] S. Dong, J. Feng, M. Fan, Y. Pi, L. Hu, X. Han, M. Liu, J. Sun, Recent developments in heterogeneous photocatalytic water treatment using visible light-responsive photocatalysts: a review, *RSC Adv.* 5 (2015) 14610-14630.
- [31] R. Ullah, J. Dutta, Photocatalytic degradation of organic dyes with manganese-doped ZnO nanoparticles, *J Hazard Mater.* 156 (2008) 194–200.
- [32] C. A. K. Gouvêa, F. Wypych, S. G. Moraes, N. Durán, S. Peralta-Zamora, Semiconductor-assisted photodegradation of lignin, dye, and kraft effluent by Ag-doped ZnO, *Chemosphere* 40 (2000) 427–432.
- [33] M. Ahmad, E. Ahmed, Y. Zhang, N. R. Khalid, J. Xu, M. Ullah, Z. Hong, Preparation of highly efficient Al-doped ZnO photocatalyst by combustion synthesis, *Curr Appl Phys.* 13 (2013) 697–704.
- [34] S. Liu, C. Li, J. Yu, Q. Xiang, Improved visible-light photocatalytic activity of porous carbon self-doped ZnO nanosheet-assembled flowers, *Cryst Eng Comm.* 13 (2011) 2533–2541.
- [35] K. C. Barack, S. Singh, M. Aslam, D. Bahadur, Porosity and photocatalytic studies of transition metal doped ZnO nanoclusters, *Microporous Mesoporous Mater.* 134 (2010) 195–202.

- [36] F. Achouri, S. Corbel, L. Balan, K. Mozet, E. Girot, G. Medjahdi, M. Ben Said, A. Ghrabi, R. Schneider, Porous Mn-doped ZnO nanoparticles for enhanced solar and visible light photocatalysis, *Mater Des.* 101 (2016) 309–316.
- [37] J. B. Zhong, J. Z. Li, J. Zeng, X. Y. He, W. Hu, Y. C. Shen, Enhanced photocatalytic performance of Ga³⁺-doped ZnO, *Mater. Res. Bull.* 47 (2012) 3893-3896.
- [38] S. Bhatia, N. Verma, R. K. Bedi, Effect of aging time on gas sensing properties and photocatalytic efficiency of dye on In-Sn co-doped ZnO nanoparticles, *Mater. Res. Bull.* 88 (2017) 14-22.
- [39] J. C. Sin, S. M. Lam, K. T. Lee, A. Mohamed, Preparation and photocatalytic properties of visible light-driven samarium-doped ZnO nanorods, *Ceram Int.* 39 (2013) 5833-5843.
- [40] I. Zgura, N. Preda, G. Socol, C. Ghica, D. Ghica, M. Enculescu, I. Negut, L. Nedelcu, L. Frunza, C. P. Ganea, S. Frunza, Wet chemical synthesis of ZnO-CdS composites and their photocatalytic activity, *Mater. Res. Bull.* 99 (2018) 174-181.
- [41] R. Vogel, P. Hoyer, H. Weller, Quantum-Sized PbS, CdS, Ag₂S, Sb₂S₃, and Bi₂S₃ Particles as Sensitizers for Various Nanoporous Wide-Bandgap Semiconductors, *J Phys Chem.* 98 (1994) 3183–3188.
- [42] F. Achouri, S. Corbel, A. Aboulaich, L. Balan, A. Ghrabi, M. Ben Said, R. Schneider, Aqueous synthesis and enhanced photocatalytic activity of ZnO/Fe₂O₃ heterostructures, *J Phys Chem Solids* 75 (2014) 1081–1087.

- [43] I. Unlu, J. W. Soares, D. M. Steeves, J. E. Whitten, Photocatalytic Activity and Fluorescence of Gold/Zinc Oxide Nanoparticles Formed by Dithiol Linking, *Langmuir* 31 (2015) 8718–8725.
- [44] S. Khanchandani, S. Kundu, A. Patra, A. K. Ganguli, Band Gap Tuning of ZnO/In₂S₃ Core/Shell Nanorod Arrays for Enhanced Visible-Light-Driven Photocatalysis, *J Phys Chem C* 117 (2013) 5558–5567.
- [45] X. Liu, H. Chu, J. Li, L. Niu, C. Li, H. Li, L. Pan, C. Q. Sun, Light converting phosphor-based photocatalytic composites, *Catal Sci Technol*. 5 (2015) 4727-4740.
- [46] J. Wang, J. Li, B. Liu, Y. P. Xie, G. X. Han, Y. Li, L. Q. Zhang, X. D. Zhang, Preparation of nano-sized mixed crystal TiO₂-coated Er³⁺:YAlO₃ by sol-gel method for photocatalytic degradation of organic dyes under visible light irradiation, *Water Sci Technol*. 60 (2009) 917-926.
- [47] H. G. Yang, Z. W. Dai, Z. W. Sun, Upconversion luminescence and kinetics in Er³⁺:YAlO₃ under 652.2 nm excitation, *J Lumin*. 124 (2007) 207-212.
- [48] J. Wang, Y. P. Xie, Z. H. Zhang, J. Li, X. Chen, L. Zhang, R. Xu, X. D. Zhang, Photocatalytic degradation of organic dyes with Er³⁺:YAlO₃/ZnO composite under solar light, *Sol Energy Mater Sol Cells* 93 (2009) 355–361.
- [49] H. Chu, X. J. Liu, J. Liu, W. Lei, J. Li, T. Wu, P. Li, H. Li, L. Pan, Down-conversion phosphors as noble-metal-free co-catalyst in ZnO for efficient visible light photocatalysis, *Appl Surf Sci*. 391 (2017) 468-475.
- [50] X. Liu, L. Pan, J. Li, K. Yu, Z. Sun, C. Q. Sun, Light down-converting characteristics of ZnO–Y₂O₂S:Eu³⁺ for visible light photocatalysis, *J Colloid Interface Sci*. 404 (2013) 150–154.

- [51] X. Liu, X. Wang, H. Li, J. Li, L. Pan, J. Zhang, G. Min, Z. Sun, C. Sun, Enhanced visible light photocatalytic activity of ZnO doped with down-conversion NaSrBO₃:Tb³⁺ phosphors, Dalton Trans. 44 (2015) 97-103.
- [52] X. Liu, X. Wang, H. Li, L. Pan, T. Lv, Z. Sun, C. Sun, Microwave-assisted synthesis of ZnO–Y₃Al₅O₁₂:Ce³⁺ composites with enhanced visible light photocatalysis, J Mater Chem. 22 (2012) 16293-16298.
- [53] A. Aboulaich, C. M. Tilmaciu, C. Merlin, C. Mercier, H. Guilloteau, G. Medjahdi, R. Schneider, Physicochemical properties and cellular toxicity of (poly)aminoalkoxysilanes-functionalized ZnO quantum dots, Nanotechnology, 23 (2012) 335101-335110.
- [54] S. Brunauer, P. H. Emmett, E. Teller, Adsorption of gases in multimolecular layers, J Am Chem Soc. 60 (1938) 309–319.
- [55] E. P. Barrett, L. G. Joyner, P. P. Halenda, The determination of pore volume and area distributions in porous substances. I. Computations from nitrogen isotherms, J Am Chem Soc. 73 (1951) 373–380.
- [56] B. D. Cullity, S. R. Stock, Elements of X-Ray Diffraction. 3rd Edition Prentice Hall: New York, 2001, pp. 149-151.
- [57] K. S. W. Sing, D. H. Everett, R. A. W. Haul, L. Moscou, R. A. Pierotti, J. Rouquerol, T. Siemieniewska, Reporting physisorption data for gas/solid systems with special reference to the determination of surface area and porosity, Pure Appl. Chem. 57 (1985) 603–619.

- [58] G. Hitkari, S. Singh, G. Pandey, Synthesis, characterization and visible light degradation of organic dye by chemically synthesized ZnO/ γ -Fe₃O₄ nanocomposites, *Int. J. Adv. Res. Sci. Eng. Technol.* 4 (2017) 3960-3965.
- [59] A-T. T. Do, H. T. Giang, T. T. Do, N. Q. Pham, G. T. Ho, Effects of palladium on the optical and hydrogen sensing characteristics of Pd-doped ZnO nanoparticles, *Beilstein J. Nanotechnol.* 5 (2014) 1261–1267.
- [60] M. Velásquez, I. P. Santander, D. R. Contreras, J. Yáñez, C. Zaror, R. A. Salazar, M. Pérez-Moya, H. D. Mansilla, Oxidative degradation of sulfathiazole by Fenton and photo-Fenton reactions, *J Environ Sci Health A Tox Hazard Subst Environ Eng.* 49 (2014) 661–670.
- [61] C. Bohne, K. Faulhaber, B. Giese B, A. Hafner, A. Hofmann, H. Ihmels, A. K. Kohler, S. Pera, F. Schneider, M. A. Sheepwash, Studies on the Mechanism of the Photo-Induced DNA Damage in the Presence of Acridizinium Salts Involvement of Singlet Oxygen and an Unusual Source for Hydroxyl Radicals, *J Am Chem Soc.* 127 (2005) 76–85.
- [62] B. I. Ipe, M. Lehning, C. M. Niemeyer, On the Generation of Free Radical Species from Quantum Dots, *Small* 1 (2005) 706–709.
- [63] R. Chahboune, H. Mountacer, M. Sarakha, Application of liquid chromatography/electrospray ionization tandem mass spectrometry for the elucidation of hydroxyl radical oxidation of metsulfuron methyl and related sulfonylurea pesticide products: evidence for the triazine skeleton scission, *Rapid comm. Mass. Spectrom.* 29 (2015) 1370-1380.